Available online at www.sciencedirect.com
SCIENCE DIRECT
Applied Catalysis B: Environmental 61 (2005) 98–106
APPLIED CATALYSIS B: ENVIRONMENTAL
www.elsevier.com/locate/apcatb

Dynamic behaviour of activated carbon catalysts during ozone decomposition at room temperature

Challapalli Subrahmanyam, Dmitri A. Bulushev, Lioubov Kiwi-Minsker *

Ecole Polytechnique Fédérale de Lausanne (EPFL), LGRC, CH-1015 Lausanne, Switzerland

Received 13 January 2005; received in revised form 18 April 2005; accepted 19 April 2005
Available online 23 May 2005

Abstract

The catalytic decomposition of ozone (200–1600 ppm) to molecular oxygen was investigated over activated carbons in the form of woven fibre fabrics (ACF) or granules (ACG) at room temperature. The dynamics of carbon activity was characterised by two distinct regions. First the ''high activity'' towards ozone decomposition was observed, which was mainly due to chemical interaction of ozone with carbon. This interaction resulted in the formation of oxygen containing surface groups on carbon until saturation. Then the conversion was sharply decreased and carbons went to ''low activity'' region. The ozone decomposition to molecular oxygen takes place in this region following a catalytic route. The carbon activity in dry atmosphere was compared with the activity in the presence of water vapour and NO_x. Water vapour diminished the catalytic activity, but in the presence of NO_x carbons were observed to be more active due to the change in the C-surface functionality. The surface functional groups were modified in two ways: by boiling in diluted HNO_3 or by thermal treatment in He at temperatures up to 1273 K. The acid pre-treatment was found to increase the activity of carbons under the quasi steady-state, while the thermal treatment at 1273 K renders catalysts with lower activity. The ozone decomposition toward gasification of carbon producing CO_x took place with the selectivity less then 25%. The catalysts were characterised by temperature-programmed decomposition of surface functional groups, X-ray photo-electron and IR-spectroscopy. Mechanistic aspects of the reaction are discussed.

Keywords: Activated carbon; Ozone decomposition; Surface functional groups; Structured fibre catalyst; Gasification of carbon; Temperature-programmed decomposition; XPS; FT-IR

1. Introduction

Ozone in upper levels of the atmosphere protects the Earth's surface against harmful UV radiation, but on the ground level it is toxic in high concentrations is an air contaminant [1–2]. Ozone in concentration >0.1 ppm causes severe health problems to humans like headaches, throat irritation and damage to the mucous membranes [3]. Low concentrations of ozone (<2 ppm) appear in the atmosphere due to ultraviolet radiation and electric discharges. At low concentrations, ozone can be removed easily by various adsorbents and catalysts. However, photocopier machines, laser printers and plasma reactors produce ozone in higher concentrations up to 2000 ppm. Therefore, design and testing of innovative catalysts to abate higher concentrations of ozone is warranted.

Catalytic ozone decomposition at room temperature is advantageous as compared to the thermal decomposition in view of energy saving since there is no need in this case to heat large volumes of air [4–5]. Noble metals like Pt, Rh, Pd and transition metal oxides including Mn, Co, Cu, Fe, and Ni supported on γ-Al_2O_3, SiO_2, TiO_2 have been used to catalyze this reaction [5–12]. Activated carbon is also used for the destruction of ozone by adsorptive decomposition giving oxygen. Although many reports deal with mechanistic aspects of ozone decomposition on carbon, the conclusions of these studies show many discrepancies. Both non-catalytic and catalytic routes of ozone decomposition on activated carbon have been reported [13–14]. The use of activated carbon is simple and not expensive, but they have low mechanical strength. Recently, activated

* Corresponding author. Tel.: +41 21 693 3182; fax: +41 21 693 3190.
E-mail address: lioubov.kiwi-minsker@epfl.ch (L. Kiwi-Minsker).

0926-3373/$ – see front matter © 2005 Elsevier B.V. All rights reserved.
doi:10.1016/j.apcatb.2005.04.013

carbon fibres (ACF) in the form of woven fabrics were shown to be an alternative to granular activated carbons. They are easy to handle without dusting and produce a low pressure drop during the gas passage in the reactor through this catalyst bed. Moreover, ACFs have a high mechanical stability and have been used successfully in wastewater treatment for recovery of heavy metals [15–17]. Activated carbon possesses surface functional groups, whose concentration can be controlled by pre-treatment in dilute nitric acid [18–20]. Metals or metal oxides were also deposited on ACF in the form of nano-particles. This leads to the structured catalyst effective for liquid-phase hydrogenations, and has been used for low temperature oxidation of carbon monoxide [20–24].

This study is aimed at the development of structured ACF catalysts for ozone decomposition. The dynamics of carbon activity under dry and humid conditions is investigated. The effect of the ACF pre-treatment and the presence of nitrogen oxides (NO_x) in the stream have also been studied. The carbons morphology and chemical properties were characterized via BET specific surface area, FT-IR, XPS and temperature-programmed desorption. The information obtained is related to the mechanistic aspects of ozone decomposition.

2. Experimental

2.1. Materials

Granulated activated carbon (ACG) with particles of 0.5 mm diameter (Darko, Aldrich, 660 $m^2\,g^{-1}$) and activated carbon fibres synthesized from polyacrylnitrile (ACF) in the form of woven fabrics (AW1101, KoTHmex, Taiwan Carbon Company, 880 $m^2\,g^{-1}$) were used during this study. The ACF and ACG underwent different pre-treatments: were boiled in 15% HNO_3 for 1 h, rinsed in water and dried in air at room temperature (denoted as ACF(HNO_3) and ACG(HNO_3)). The ACF(HNO_3) sample was also calcined in He at 1273 K for 30 min (ACF(HNO_3, 1273 K)). The specific surface area of ACF was observed to increase after the treatment in HNO_3 up to 950 $m^2\,g^{-1}$ and to decrease after calcination in He to 660 $m^2\,g^{-1}$. It is known that treatment in diluted HNO_3 does not affect the physical morphology of the carbons, but modifies their surface chemical properties [29]. The change in the BET surface area after acid treatment was small increasing from 880 up to 950 $m^2\,g^{-1}$, and might be due to the creation of surface defects. However, the severe treatment at 1273 K in He changes slightly the texture properties, reflecting in the decrease of the BET surface area (950–660 $m^2\,g^{-1}$).

2.2. Catalyst characterization

The specific surface area (SSA) of the catalysts was measured by N_2 adsorption–desorption isotherms at 77 K using BET method in a Sorptomatic 1990 instrument (Carlo Erba). The samples were out-gassed at 523 K for 2 h using a turbo molecular pump, which gives a vacuum higher than 10^{-6} Torr before the measurement.

Oxygen containing functional groups on the ACF surface were characterised by temperature programmed decomposition (TPD) in He (50 ml min^{-1}, temperature ramp 10 K min^{-1}) using a Micrometrics AutoChem 2910 analyzer. In a typical TPD run, 0.06 g of the catalyst was placed in a quartz plug-flow reactor. The TPD products were analyzed by a Thermostar-200 quadrupole mass spectrometer (Pfeiffer Vacuum) calibrated with gas mixtures of known compositions. The intensity of the following peaks was monitored simultaneously: 2, 4, 15, 18, 28, 30, 32 and 44 m/e. Before the TPD runs the charged reactor was purged with He for 20 min at room temperature.

FT-IR studies were performed in the transmittance mode in ambient air using a Perkin-Elmer FT-IR 2000 spectrometer equipped with a MCT detector. A mixture of KBr with ACF (100:1) was milled in an agate mortar manually before the preparation of pellets. A pellet with a mixture of KBr with ACF(HNO_3, 1273 K) was used as a reference. The spectra were obtained by averaging of 64 scans with 4 cm^{-1} resolution.

The surface composition of the ACF samples was measured by XPS using an Axis Ultra ESCA system (Kratos, Manchester) with monochromated Al Kα radiation (1486.6 eV). The binding energy (BE) scale was referenced against the C1s = 285.0 eV line.

2.3. Apparatus and procedure

The ozone decomposition was studied in a set-up equipped by a quartz tubular reactor. A reactor with the 300 mm length and 10 mm diameter was used for the catalyst charge 1.0 and 0.3 g, whereas a reactor with 300 mm length and 5 mm diameter was used for low catalyst charge of 0.03 g. The gases supply was controlled by flow-controllers. Ozone was produced either from air or from oxygen diluted in helium (21 vol%) by passing through an ozone generator (Fischer-OZ II). In the case of air, the gas mixture contained also NO_x gases, which are formed in ozone generators from nitrogen of the air. To study the influence of humidity, the gas mixture containing ozone was saturated with water vapour by passing through a bubble column at 300 K providing a H_2O concentration of ~35,600 ppm.

The activity measurements were performed with the catalyst loading between 0.03–0.3 g, at flow rate of the gas mixture of 0.5–1.0 l min^{-1}, with ozone concentration of 200 or 1600 ppm. The volumetric space velocities were 1×10^6 and $1 \times 10^5\,h^{-1}$ for 0.03 and 0.3 g of the catalysts, respectively. The concentrations of ozone are far below the explosion limit for ozone in contact with activated carbon (20 g m^{-3} or ~9300 ppm).

In a typical experiment, the catalyst was heated at 473 K under a flow of helium for 2 h before the reaction to remove

the adsorbed water and volatile impurities, and then cooled down to room temperature. The ozone concentrations at the reactor inlet and outlet were monitored by an ozone detector API-Model-450 NEMA with a sensitivity of 0.1 ppm. The Beer-Lambert's relation is used in this monitor to determine the ozone concentration based on the absorption in UV-region. An infrared detector (Siemens, Ultramat-21P) with a sensitivity of 50 ppm was used to identify if CO_2 and CO are formed during the reaction. Likewise, a NO_x detector (Eco Physics CLD 822) was used to identify the nitrogen oxides formed when air was used as a reactant during ozone generation.

3. Results

3.1. Ozone decomposition on granulated ACG in comparison with ACF

Fig. 1 presents the comparative activities of granulated active carbons (ACG) and activated carbon fibre (ACF) during the decomposition of ozone generated from air under humid conditions. It can be seen that the initial activity of ACG and ACF is similar in spite of the fact that chemical composition of the carbons is different. The ACF contains structural nitrogen (∼4%) due to the polyacrylnitrile used during its preparation. AGC was found to contain a lower content of nitrogen (∼0.5%). As ACG and ACF showed the same catalytic activity, it can be assumed that this structural nitrogen did not contribute meaningfully to ozone decomposition (Fig. 1). The conversion of ozone decomposition was seen to decrease over both non-treated catalysts, but for acid treated samples a quasi-steady state seems to be attained. Since ACG and ACF showed the same activity, the experiments were carried out only with ACF catalysts during the rest of this work.

The formation of NO_x was observed in the stream with a maximum of 10 ppm during the ozone generation from air. In order to evaluate the effect of NO_x and H_2O on ozone decomposition, a higher concentration of ozone (∼1600 ppm) was used for this purpose.

3.2. Initial activity of ACF during ozone decomposition

As has been mentioned above, NO_x gases might affect ozone decomposition over ACF. To investigate this, ozone was generated from air or alternatively from pure oxygen and its decomposition was followed over ACF catalyst with a charge of 0.03 g. Fig. 2 shows that the initial activity of ACF was higher in dry conditions (conversion ∼90%) as compared to humid conditions (conversion ∼70%). However, these catalysts were very quickly deactivated during ∼4 min on stream showing low quasi steady-state activity with conversion of 5–10%. Since in these experiments the initial ozone concentration was 1600 ppm and the amount of the catalyst was only 0.03 g, it is not possible to evaluate the influence of the reaction conditions on the steady-state activity. Therefore, a bigger amount (0.3 g) of the ACF catalyst was used in further experiments to study the catalyst dynamics in detail.

3.3. Dynamics of ACF activity during ozone decomposition: influence of water

Fig. 3a and b present the activity dynamics of the ACF samples (0.3 g) during ozone decomposition under dry and humid conditions, respectively. Ozone was produced from pure oxygen (21 vol% in He), and no NO_x was observed in the ozone containing stream. Two distinct activity regions were observed. In the first region, the decomposition was fast with a conversion close to 100%. In the second region, ozone decomposition was slower, with a conversion below 20%. The transition between the first and the second region takes place steeply at the breakthrough point. This dynamics suggest that at least two different processes are responsible for ozone decomposition.

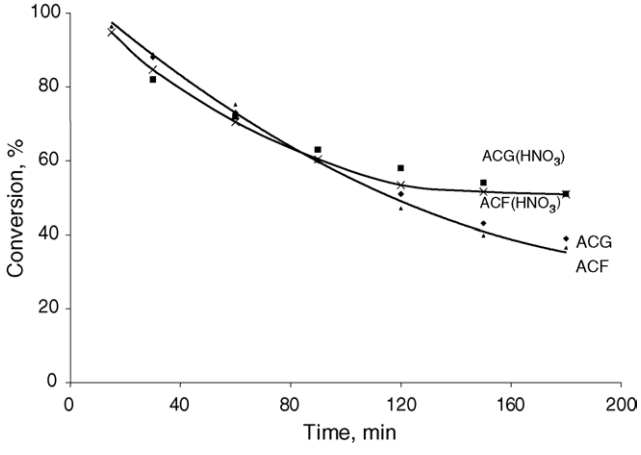

Fig. 1. Comparative activities before and after HNO_3 treatment of ACG and ACF catalysts (0.2 g) during ozone decomposition in the presence of NO_x, under humid conditions; 200 ppm of ozone, total flow 0.5 l min^{-1}.

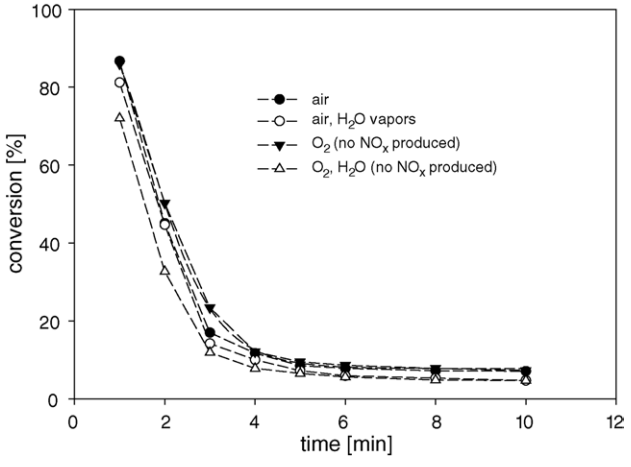

Fig. 2. Activity of ACF catalyst (0.03 g) for the decomposition of ozone produced from air (NO_x present in O_3 stream) and from oxygen; 1600 ppm of ozone, total flow 1.0 l min^{-1}.

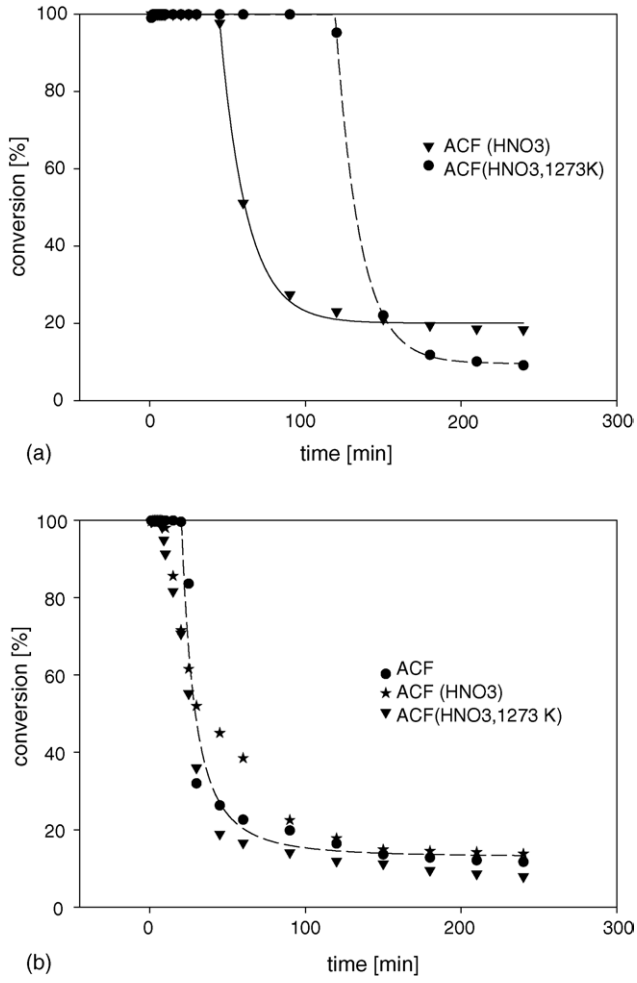

Fig. 3. Activity of ACF catalyst (0.3 g) for decomposition of ozone produced from oxygen in (a) dry conditions and in (b) humid conditions; 1600 ppm of ozone, total flow 1.0 l min^{-1}.

It is seen in Fig. 3a that under dry conditions the steep decrease from 100% to steady-state ozone conversion starts much earlier (∼50 min) with the ACF(HNO_3) catalyst as compared to the ACF(HNO_3, 1273 K). In the latter case, the ozone breakthrough time is close to ∼120 min. This suggests that a different amount of functional groups on the carbon surface is responsible for the different length of initial period of high activity observed during ozone decomposition. As it will be shown later, these groups are already present in large amounts on the carbon surface due to acid treatment (in the ACF(HNO_3) fresh catalyst). This provides a shorter initial period before the breakthrough compared to the ACF(HNO_3, 1273 K) sample. The functional groups on the surface prevent the ozone molecules from interaction with the carbon. In spite of the longer breakthrough time on the ACF(HNO_3, 1273 K) catalyst, it shows a two-fold lower steady-state activity after 4 h on stream as compared to the ACF(HNO_3) catalyst.

From the steady-state conversions attained, the specific reaction rates were calculated for ACF(HNO_3) (950 m^2 g^{-1}) and ACF(HNO_3, 1273 K) (660 m^2 g^{-1}) catalysts being 8×10^{-10} and 6×10^{-10} mol m^{-2} s^{-1}, respectively. These values are in the range of the reported data for the steady-state activities of various carbons (10^{-9} to 10^{-11} mol m^{-2} s^{-1}) [5]. The difference in the specific reaction rate with those obtained from the other studies can be attributed to the different conditions (concentration of ozone, flow rate, etc.) as well as to the differences between carbon samples [1,5]. Nevertheless, the rates obtained in the present study are lower as compared to the rates reported for oxide catalysts [5]. An important observation is that the formation of CO, CO_2 is not found within the sensitivity level of detection at 50 ppm. Hence, the steady-state ozone decomposition to oxygen was assigned mainly to a catalytic process due to carbon.

Fig. 3b presents the comparative activities of the ACF catalysts for ozone decomposition in the presence of water vapour (relative humidity >90%). Under these conditions, the decomposition of ozone followed the same trend as in dry conditions. The rapid decomposition in the first region is followed by a lower rate of ozone decomposition after the breakthrough point. Important is that the breakthrough time becomes smaller in the presence of water vapour as compared to reaction in a dry atmosphere (Fig. 3a). The negative effect of water vapour may be due to the blockage of the active carbon sites by adsorbed water molecules.

However, in the presence of water vapour the ACF(HNO_3) catalyst showed the highest steady-state activity beyond 4 h in ozone stream as compared to the ACF and ACF(HNO_3, 1273 K) catalysts. This is partially explained by the difference in the BET surface areas (Table 1). The SSA of carbon is known to decrease after the interaction with ozone [13,25–27].

3.4. Dynamics of ACF activity during ozone decomposition: influence of NO_x

As it was mentioned above, ozone generation from air is accompanied by NO_x formation from the N_2 present in air. Fig. 4 presents the comparative activities of the ACF(HNO_3, 1273 K) catalyst for the decomposition of ozone in (a) dry ozone, (b) dry ozone with NO_x (c) humid ozone with NO_x and (d) humid ozone. It is seen that two regions of the catalyst activities towards ozone decomposition exist independently on the applied conditions. After 4 h on stream, the steady-state conversion of ozone in the presence

Table 1
Concentrations of CO_2 and CO evolved from the ACF samples during TPD performed before and after ozone decomposition for 12 h

Sample	CO_2 (mmol g^{-1})	CO (mmol g^{-1})
ACF (880 m^2 g^{-1})	0.43	2.6
ACF after O_3	2.4	3.1
ACF(HNO_3) (950 m^2 g^{-1})	1.3	3.6
ACF(HNO_3) after O_3	2.3	3.7
ACF(HNO_3, 1273 K) (660 m^2 g^{-1})	0	0.34
ACF(HNO_3, 1273 K) after O_3	1.6	1.8

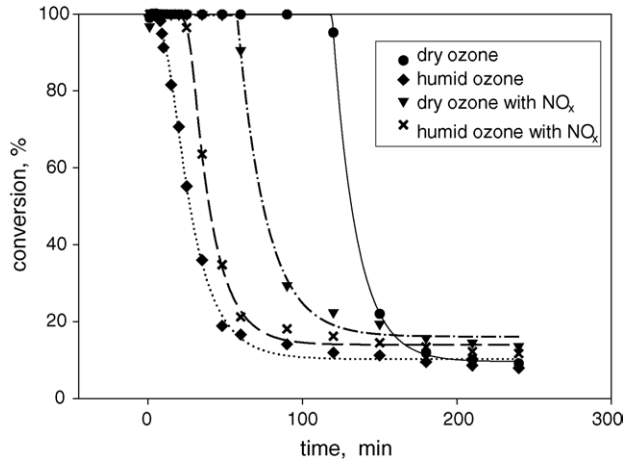

Fig. 4. Effect of the presence of NO_x and water vapour in the stream on the activity of ACF(HNO_3, 1273 K) catalyst (0.3 g) during ozone decomposition; 1600 ppm of ozone, total flow 1.0 l min^{-1}.

of NO_x is 1.5 times higher than in the absence of NO_x. This suggests that the NO_x reaction with ozone contributes to the catalytic route of ozone decomposition to oxygen. Similar observations were made for the ACF(HNO_3) and ACF catalysts. Thus, in variance with the effect of water vapour (Fig. 4), the presence of NO_x gases increased the catalytic ozone decomposition.

A comparison of the activity of different samples was performed in the presence of NO_x gases in humid atmosphere over ACF(HNO_3), ACF original and ACF(HNO_3, 1273 K) for a long period up to 12 h (not shown). It was observed that even in the presence of NO_x gases, ozone decomposition activities followed the same trend like in Fig. 3b (ozone without NO_x gases), where acid treated catalyst, ACF(HNO_3), showed the highest steady-state conversion (~25%) after 12 h on stream. The original ACF was more active than ACF(HNO_3, 1273 K) under the same experimental conditions. Moreover, the ACF(HNO_3, 1273 K) catalyst showed strong deactivation during the reaction after 12 h.

In the above experiments, when working with 0.3 g of the ACF sample, gasification of carbon to CO_x was not observed within the CO_x detector sensitivity of 50 ppm in both high and low activity regions. In order to ensure this observation, ozone decomposition was followed for the high charge of the catalyst (1.0 g) with a relative humidity ~70% for a period of 12 h (not shown). The dynamics of ozone decomposition remained the same with the break-through time ~5 h. The conversion decreased at this moment from 100% down to 45% and remained constant afterwards. Interestingly, that in high and low activity regions small amount of CO_2 and CO (from 150 to 400 ppm) was detected. The selectivity of ozone decomposition to CO_x was initially ~25% and then decreased slowly (after 600 min) to ~15%. It was assumed that one ozone molecule forms one CO molecule, whereas two ozone molecules are needed to form one molecule of CO_2 [5]. This indicates that only a part of ozone was used to produce CO_x, and most of it was decomposed to molecular oxygen over the carbon surface via a catalytic route.

3.5. Characterization of surface functional groups on ACF catalysts

Characterization of the ACF samples was performed before and after the ozone decomposition for 12 h in humid atmosphere and in the presence of NO_x formed in ozone generator when using air.

3.5.1. Temperature programmed decomposition (TPD)

Fig. 5 presents the TPD profiles of different samples. The TPD of the ACF(HNO_3, 1273 K) fresh catalyst does not show any CO_2 evolution. CO is evolved in a small amount only at high temperatures. Hence, the fresh sample almost does not contain any oxygen functional groups. The ozone decomposition on this sample leads to the formation of large amount of oxygen functional groups on the surface, which gives CO_2 and CO during the TPD run (Fig. 5). The profiles of the CO_2 and CO peaks were broad indicating decomposition of several types of the oxygen containing functional groups.

The release of CO_2 was observed to start at lower temperature than CO. The low temperature peak of the CO_2 evolution (<540 K) is mainly due to the carboxylic groups decomposition [28–29]. Decomposition of acid derivatives

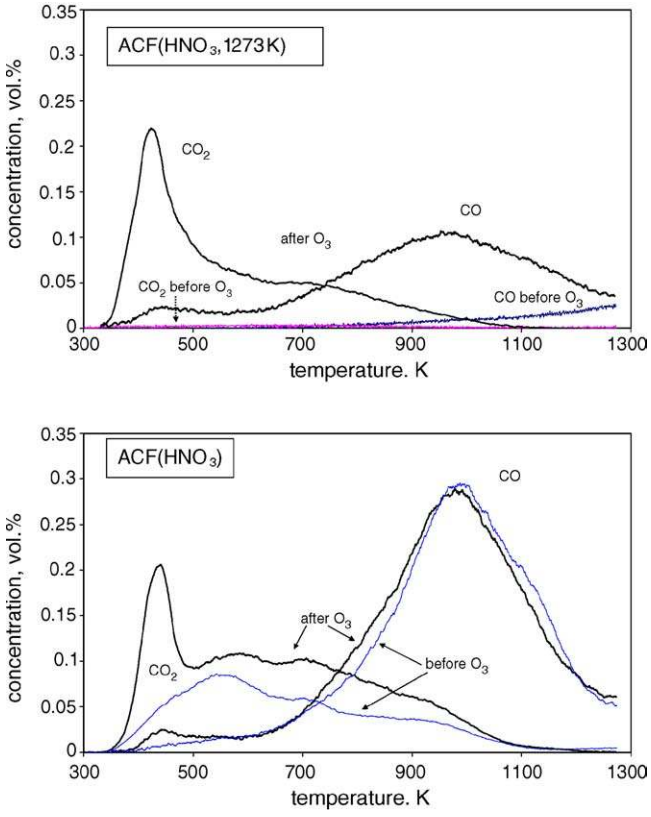

Fig. 5. TPD profiles obtained with the ACF samples (0.06 g) before and after ozone decomposition for 12 h.

like lactol and lactone groups takes place at high temperature (463–923 K), whereas anhydride groups decompose with simultaneous CO and CO_2 formation at 650–950 K. Phenolic and carbonyl/quinone groups have been reported to be responsible for CO evolution at >800 K. Hydrogen formation was observed at temperatures higher than 960 K.

The TPD profile of the ACF(HNO_3) indicates that the fresh sample already contains several types of functional groups (Fig. 5). The amount of the groups evolving CO_2 is higher than in the ACF sample non-treated in HNO_3 (Table 1). The ozone decomposition performed over the ACF(HNO_3) does not change the CO profile (Fig. 5). A strong peak at 423 K was observed for the CO_2 curve. After ozone decomposition, the profiles for the ACF(HNO_3, 1273 K) and ACF(HNO_3) samples (Fig. 5) become qualitatively similar. However, the total concentration of the produced CO and CO_2 is lower for ACF(HNO_3, 1273 K) (Table 1). This could be partly explained by a lower specific surface area of the sample.

Table 1 shows that the decomposition of ozone over carbon catalysts leads to the formation of the surface groups evolving CO_2 during the TPD run. This was observed for all the samples studied. CO containing groups are formed only on the samples, which do not contain these groups before the interaction with ozone. If the samples have been already saturated with the CO evolving groups, like the ACF and ACF(HNO_3), their concentration almost does not change during the ozone decomposition reaction.

The amounts of functional groups formed during ozone reacting with different ACFs and determined by TPD (Table 1) allow estimating the time before the break-through point. This is the time necessary to form these groups under the reaction conditions used. It was considered that the formation of the groups giving CO and CO_2 in TPD is a result of carbon reacting with one and two ozone molecules respectively. The conversion of ozone to these groups was taken equal to 100%. The initial amount of the groups present on the ACF before reaction was subtracted from the ones determined after the ozone reaction. Thus, for the experiments shown in Fig. 2 about 2 min are necessary to form the functional groups. This is in line with the observed time of break-through (less than 3 min). From the experiments shown in Fig. 3b, the calculations gave around 20 min for the ACF and ACF(HNO_3, 1273 K) samples and 9 min for the ACF(HNO_3) one. In accordance, the experimental break-through observed (high activity region) was about 30 min. Hence, it suggests that the initial high conversion of ozone decomposition is due to its participation in the formation of functional groups on the carbon surface. FT-IRS and XPS were used to discriminate the nature of these groups.

3.5.2. FT-IR spectroscopy

FT-IR spectra for the ACF samples after ozone decomposition are shown in Fig. 6. All spectra are related to the one of the ACF(HNO_3, 1273 K) sample, which almost does not contain functional groups (Table 1, Fig. 5).

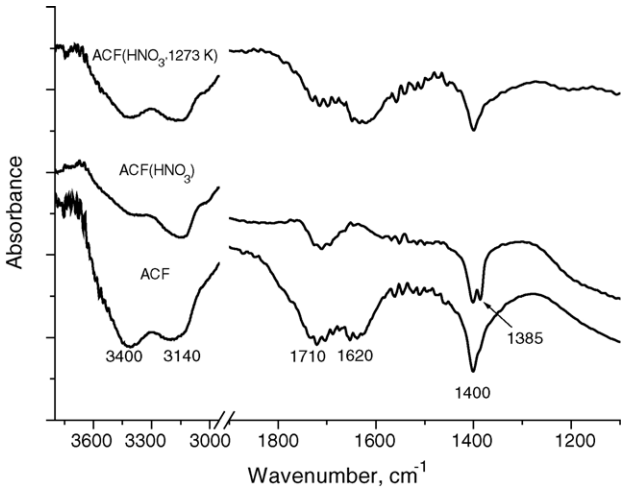

Fig. 6. FT-IR spectra of the ACF samples obtained after the ozone decomposition for 12 h.

It is seen that after the decomposition the bands at 3000–3700, 1710–1720, 1630 and 1400/1385 cm^{-1} appear in the IR spectrum. The band at 1710 cm^{-1} is assigned to C=O stretching in carboxylic groups [30]. The concomitant appearance of the OH stretching at 3130 and 3430 cm^{-1} associated with H-bonded hydroxyls involved in carboxylic and phenolic groups is observed. Lactone groups may contribute to the 1710–1740 cm^{-1} peaks also [30,31]. The band at around 1630 cm^{-1} is assigned to quinones [26,27] or to the carbon aromatic framework vibration (C=C) induced by the oxidation of ACF [30–31]. This band is not found for the ACF(HNO_3) sample. No carboxylic anhydride groups (1830, 1760 cm^{-1}) were observed.

One or two bands at around 1400 cm^{-1} are seen for all samples after ozone decomposition (Fig. 6). Their intensities before the reaction are much lower. An intensive sharp band at 1385 cm^{-1} was observed for the ACF(HNO_3). It is assigned to nitrate (NO_3^-) species formed because of the carbon treatment by nitric acid (32). However, the presence of these species in other samples, contributing as a shoulder to the band at 1400 cm^{-1} may not be excluded. In these samples, the nitrate could be produced from NO_x gases formed from nitrogen in the ozone generator. Similar assignment was performed earlier [32]. Interesting is that small desorption of NO was observed during TPD runs for the ACF(HNO_3) and ACF samples, but not in the case of the ACF(HNO_3, 1273 K) sample, whether before or after ozone decomposition.

The band at 1400 cm^{-1} is typical for all samples after the ozone decomposition and can be attributed to different species. For carboxyl-carbonates, lactone, nitrites, some nitrates species the bands at around 1500–1650 cm^{-1} should be observed and were found on ACF(HNO_3, 1273 K) and ACF. However, they were not observed in the spectrum of the ACF(HNO_3) after ozone decomposition (Fig. 6), showing the bands at 1400, 1385 cm^{-1}. The intensity of

the 1400 cm^{-1} band increased after ozone decomposition simultaneously to the band of the hydroxyl groups (3000–3700 cm^{-1}) (Fig. 6). Hence the band at 1400 cm^{-1} is assigned mainly to hydrogen bonded hydroxyl groups (δ(OH)) in accordance to the result reported in [33].

3.5.3. XPS

Selected ACF samples were studied by XPS and the spectra are presented in Fig. 7. In the sample treated at 1273 K (ACF(HNO_3, 1273 K)) the surface oxygen content was found to be negligible (Table 2). This is in agreement with the TPD data (Table 1, Fig. 5). The concentration of the oxygen functional groups increased considerably after HNO_3 treatment or ozone decomposition. This results further support the TPD and FT-IRS experimental data (Table 1, Figs. 5 and 6).

The analysis of the C1s band showed that no carboxylic/ester groups (289.1–289.2 eV, Table 3) were present in the ACF(HNO_3, 1273 K) sample. This is in agreement with the absence of CO_2 in TPD runs for this sample. However, carboxylic/ester groups were observed in the HNO_3 treated sample (ACF(HNO_3)) and with two times higher concentration for the ACF(HNO_3, 1273 K) sample after ozone decomposition (Table 3). This is in line with the presence of the large CO_2 TPD peak at 423 K (Fig. 5). It was reported earlier [34] that ozone treatment of the amorphous carbon in the absence of water vapour led to the carboxylic groups' formation. The presence of water vapour may facilitate this process.

The discrimination of other groups in XPS spectra is complicated, as a lot of different species may contribute to the 286–287 eV region (Table 3). Only very thermally stable groups are observed in the C1s spectrum of the ACF(HNO_3, 1273 K) sample. Among them are ethers (C–O–C), carbonyl/quinone (C=O), phenol and C–N groups.

The presence of nitrogen was found in all samples reported in Table 2. As it was mentioned above, there are two sources for the surface nitrogen containing species: the precursor for the ACF synthesis (polyacrylnitrile) and NO_x gases formed from air N_2 in the ozone generator. It was observed that the position of the maximum in the N1s region differed. For the ACF(HNO_3, 1273 K) this peak was around 398.2 eV moving to higher binding energies (399.8–400.0 eV) after ozone decomposition. The same position (~400.0 eV) was seen for the ACF(HNO_3) sample being in line with the literature data [35]. In pyrolysed carbons like ACF(HNO_3, 1273 K) nitrogen is present in pyridinic type species. After carbon oxidation, pyrrolic type N dominates shifting the BE to higher values. These nitrogen species are assigned to structural nitrogen coming from the ACF synthesis precursor.

4. Discussion

Based on the results obtained, a mechanistic reaction scheme (Fig. 8) is suggested for low temperature ozone

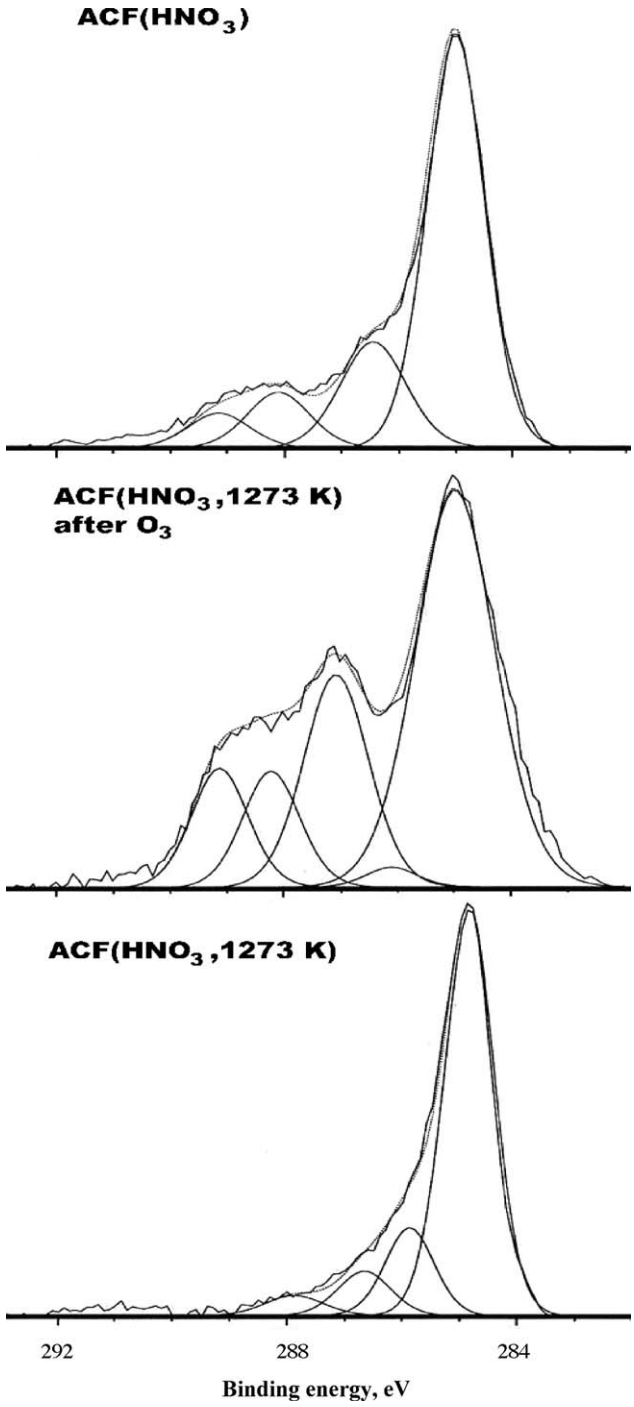

Fig. 7. XPS spectra of the ACF samples, C1s region.

Table 2
Relative surface atomic concentrations of elements in the ACF samples determined by XPS

Sample (treatment)	C (at.%)	O (at.%)	N (at.%)
ACF(HNO_3, 1273 K)	91.86	3.64	4.50
ACF(HNO_3, 1273 K) after ozone for 12 h	65.36	32.18	2.46
ACF(HNO_3)	77.57	17.08	5.35

Table 3
Results of deconvolution of the C1s band in the XPS spectra

	285.0 (eV, at.%)	286.0–286.1 (eV, at.%)	286.5–287.1 (eV, at.%)	288.0–288.2 (eV, at.%)	289.1–289.2 (eV, at.%)
Assignment	C	C–OH, C–O–R, C–N (phenols, ethers, keto-enol structures)		C=O (carbonyls, quinines)	COOR (carboxyls, esters)
ACF(HNO_3, 1273 K)	72.3	15.2	8.3	4.2	–
ACF(HNO_3, 1273 K) after ozone, 12 h	52.9	1.7	22.8	11.1	11.5
ACF(HNO_3)	65.0	–	19.3	9.7	6.0

decomposition. The formation of functional groups takes place through a chemical route. Therefore, after the reaction of ozone with the ACF treated in He at 1273 K, CO_2 and CO peaks were found in TPD. For the ACF sample treated in HNO_3, the reaction with ozone increased the amount of carboxylic groups but the amount of the groups giving CO in the TPD remained the same.

Carbon gasification to CO_x was observed only with higher charge of the catalyst (1.0 g). However, the selectivity of ozone decomposition towards formation of these groups did not exceed 25%. The gasification takes place via oxidation of functional groups (Fig. 8) as a delay was observed in the evolution of CO_x at the reactor outlet.

Ozone decomposition to molecular oxygen by catalytic route (Fig. 8) takes place with a lower rate as compared to chemical interaction. As described earlier, after rapid formation of functional groups, only a limited number of surface active sites will remain available for reaction with ozone. During the catalytic action a steady state was achieved, which can be explained as follows. The catalytic decomposition (two molecules of O_3 react to give three molecules of O_2) occurs under two different paths: (1) in the absence of NO_x (ozone produced from pure oxygen) and (2) in the presence of NO_x (ozone produced from air). Similar observation was earlier made for ozone reaction with soot, where two molecules of ozone interacted with surface sites to produce three molecules of oxygen [36,40]. In the presence of NO_x additional active sites seem to be formed on the catalyst surface. This is the reason why the presence of NO_x in the gas-phase enhances the steady state activity as suggested in Fig. 8.

Ozone reaction with ethylene may help to understand the interaction of ozone with activated carbon [13,26,27,34,37–40]. This interaction results in the formation of oxygen containing functional groups (Fig. 8). From the results of the present study it follows that the accumulation of the surface functional groups decreases the ozone decomposition rate, but does not suppress completely the reaction. The steady state conversion was observed after 12 h on stream. Since the functional groups block the carbon surface, only a limited number of surface sites can be involved in the catalytic route of ozone decomposition giving oxygen.

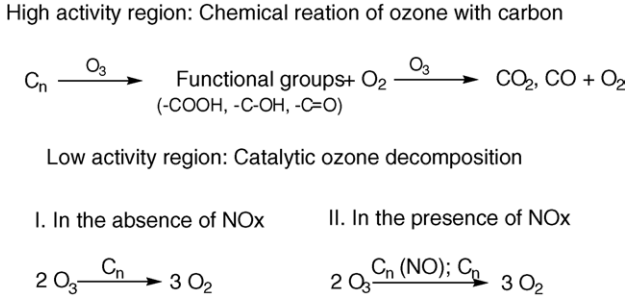

Fig. 8. Simplified scheme of ozone decomposition over activated carbons.

Humidity decreased the steady-state activity of the catalyst due to H_2O blocking the surface active sites. The presence of nitrogen species was found in all ACF samples by XPS. The NO evolution was observed in TPD only for ACF and ACF(HNO_3), but not found for ACF(HNO_3, 1273 K). The groups containing NO probably were removed during the catalyst calcinations at high temperature. FT-IRS analysis does not exclude the presence of adsorbed NO_x species after ozone decomposition for 12 h. The origin of nitrogen comes both from polyacrylnitrile (ACF precursor), and from NO_x gases formed from air nitrogen in ozone generator. In the present study, no effect of structural nitrogen (pyridinic and pyrollic groups) formed during the synthesis of ACF was observed as the activity of granulated ACG without these groups was similar to ACF (Fig. 1). However, NO_x gases provide the increase of the rates of ozone decomposition (Fig. 4). These gases in adsorbed form can catalyze the reaction as shown in Fig. 8.

It is known that the ozone decomposition can also be initiated by the existence of free electrons on the carbon surface [14]. Takeuchi et al. correlated the higher activity of nitric acid treated sample for ozone decomposition to the high electron density on carbon [14]. Matsumura et al., earlier reported that carbon sample contains free electrons whose number increases by oxidation with nitric acid as confirmed by ESR spectroscopy [14,41]. In the present study, the acid treatment increases the steady-state conversion reported in Figs. 1 and 3. Therefore, a part of ozone decomposition via catalytic route may be initiated by the surface unpaired electrons [40].

It is known that ozone interaction with carbon for a prolonged period of time can bring permanent changes to C-material, like decrease in the surface area and increase in the pore size as measured by nitrogen adsorption [13,14,26]. On exposure for a longer period, ozone partially destroys the pore network of carbon. The observed decrease in surface area is also due to the blockage of the micropore openings by newly formed functional groups preventing the access of adsorbates into the micropores [14,26].

The activities of ACF and granulated carbon (ACG) during ozone decomposition were observed to be similar (Fig. 1). The ACF creates low pressure drop during the gas passage in eventual reactor and is a dust-free structured material, which is easy to handle. Thus, the ACF in the form of woven fabric is a suitable catalyst for ozone decomposition.

5. Conclusions

(1) Effective catalyst for ozone decomposition to molecular oxygen at room temperature was developed in the form of woven fibre fabrics of active carbons (ACF).
(2) The dynamics of the ACF activity was characterised by two distinct regions: (a) the ''high activity'' of fresh catalyst mainly due to chemical interaction of ozone with carbon resulting in oxygen containing surface groups until saturation; (b) after the break-through point, the conversion sharply decreased characterizing the ''low activity'' region. The ozone decomposition to molecular oxygen takes place in this region following a catalytic route attaining the quasi steady-state.
(3) The ACF catalytic activity towards decomposition of ozone in dry atmosphere was higher than with water vapours due to partial blockage of active sites by H_2O molecules.
(4) In the presence of NO_x, the ACF catalysts were observed to be more active caused by the change in the C-surface functionality leading to the formation of new active sites.
(5) The gasification of ACF to CO_x by ozone also takes place but with selectivity of ∼10–25%. Mechanistic aspects of the decomposition of ozone on carbons are discussed and the simplified reaction scheme is proposed.

Acknowledgements

The authors acknowledge the Swiss Commission of Technology and Innovation (CTI, Bern) for financial support in the framework TOPNANO 21 program. We are also thankful to N. Xanthopoulos for XPS and E. Casali for BET surface area measurements.

References

[1] C. Heisig, W. Zhang, S.T. Oyama, Appl. Catal. B: Environ. 14 (1997) 117.
[2] T.L. Rakitskaya, A.Yu. Bandurko, A.A. Ennan, V.Ya. Paina, A.S. Rakitskiy, Micro. Meso. Mater. 43 (2001) 153.
[3] G. Gordon, Prog. Nucl. Energy 29 (1995) 89.
[4] A. Naydenov, D. Mehandjiev, Appl. Catal. A: Gen. 97 (1993) 17.
[5] S.T. Oyama, Catal. Rev. Sci. Eng. 42 (2000) 279.
[6] B. Dhandapani, S.T. Oyama, Appl. Catal. B: Environ. 11 (1997) 129.
[7] H. Einaga, S. Futumura, React. Kinet. Catal. Lett. 81 (2004) 121.
[8] S. Tong, W. Liu, W. Leng, Q. Zhang, Chemosphere 50 (2003) 1359.
[9] R. Radhakrishnan, S.T. Oyama, J. Chen, A. Asakura, J. Phys. Chem. B 105 (2001) 4245.
[10] W. Li, G.V. Gibbs, S.T. Oyama, J. Am. Chem. Soc. 120 (1998) 9041.
[11] W. Li, S.T. Oyama, J. Am. Chem. Soc. 120 (1998) 9047.
[12] W. Li, S.T. Oyama, Top. Catal. 8 (1999) 75.
[13] V.R. Deitz, J.L. Bitner, Carbon 11 (1973) 393.
[14] Y. Tekeuchi, T. Ioth, Separation Sci. Technol. 3 (1993) 168.
[15] E. Auer, A. Freund, J. Pietsch, T. Tacke, Appl. Catal. A: Gen. 173 (1998) 259.
[16] Y.G. Jia, K.M. Thomas, Langmuir 16 (2000) 1114.
[17] R.W. Fu, H.M. Zeng, Y. Lu, Mineral. Eng. 6 (1993) 721.
[18] J. Zawadzki, Carbon 18 (1980) 281.
[19] S. Haydar, C. Moreno-Castilla, M.A. Ferro-Garcia, F. Carrasco-Martin, J. Rivera-Utrilla, A. Perrard, J.P. Joly, Carbon 38 (2000) 1297.
[20] G. de la Puente, J.J. Pis, J.A. Menendez, P. Grange, J. Anal. Appl. Pyrol. 43 (1997) 125.
[21] D.A. Bulushev, L. Kiwi-Minsker, I. Yuranov, E.I. Suvorova, P.A. Buffat, A. Renken, J. Catal. 210 (2002) 149.
[22] D.A. Bulushev, I. Yuranov, E.I. Suvorova, P.A. Buffat, L. Kiwi-Minsker, J. Catal. 224 (2004) 8.
[23] S. Imamure, M. Ikebata, T. Ito, T. Ogita, Ind. Eng. Chem. Res. 30 (1991) 217.
[24] Z. Hao, D. Cheng, Y. Guo, Y. Liang, Appl. Catal. B: Environ. 33 (2001) 217.
[25] K.M. Bulanin, J.C. Lavalley, A.A. Tsyganenko, Coll. Surf. A: Physicochem. Eng. Aspects 101 (1995) 153.
[26] V.R. Dietz, J.L. Bitner, Carbon 10 (1972) 145.
[27] H. Valdes, M. Sanchez-Polo, J. Rivera-Utrilla, C.A. Zaror, Langmuir 18 (2002) 2111.
[28] H.P. Boehm, Carbon 40 (2002) 145.
[29] J.L. Figueiredo, M.F.R. Pereira, M.M.A. Freitas, J.J.M. Orfao, Carbon 37 (1999) 1379.
[30] P.E. Fanning, M.A. Vannice, Carbon 31 (1993) 721.
[31] G. Mul, J.P.A. Neeft, F. Kapteijn, J.A. Moulijn, Carbon 36 (1998) 1269.
[32] U. Zielke, K.J. Huttinger, W.P. Hoffman, Carbon 34 (1996) 983.
[33] V. Gomez-Serrano, P.M. Alvarez, J. Jaramillo, F.J. Beltran, Carbon 40 (2002) 513.
[34] D.B. Mawhinney, J.T. Yates, Carbon 39 (2001) 1167.
[35] J.R. Pels, F. Kapteijn, J.A. Moulijn, Q. Zhu, K.M. Thomas, Carbon 33 (1995) 1641.
[36] D.M. Smith, W.F. Welch, J.A. Jassim, A.R. Chughtai, D.H. Stdem, Appl. Spect. 42 (1998) 1473.
[37] V.R. Deitz, N.H. Turner, J. Phys. Chem. 75 (1971) 2718.
[38] J.S. Dusenbury, F.S. Cannon, Carbon 34 (1996) 1577.
[39] S. Stephens, M.J. Rossi, D.M. Golden, Int. J. Chem. Kin. 18 (1986) 1133.
[40] D.M. Smith, A.R. Chughtai, Coll. Surf. A. 105 (1995) 47.
[41] Y. Matsumura, J. Appl. Chem. Biotech. 25 (1975) 39.